

RSC Advances



This is an *Accepted Manuscript*, which has been through the Royal Society of Chemistry peer review process and has been accepted for publication.

Accepted Manuscripts are published online shortly after acceptance, before technical editing, formatting and proof reading. Using this free service, authors can make their results available to the community, in citable form, before we publish the edited article. This *Accepted Manuscript* will be replaced by the edited, formatted and paginated article as soon as this is available.

You can find more information about *Accepted Manuscripts* in the [Information for Authors](#).

Please note that technical editing may introduce minor changes to the text and/or graphics, which may alter content. The journal's standard [Terms & Conditions](#) and the [Ethical guidelines](#) still apply. In no event shall the Royal Society of Chemistry be held responsible for any errors or omissions in this *Accepted Manuscript* or any consequences arising from the use of any information it contains.



Journal Name

ARTICLE

HF radiofrequency exposure partially restores dynamics of model membranes containing carbon nanotubes.

G. Nugue^a, S. Dekali^a, F. Bourbon^a, L. Seleck^{b,c}, A. Laisné^d, J.C. Debouzy^{a,b}, D. Crouzier^{a,b}

Received 00th January 20xx,
Accepted 00th January 20xx

DOI: 10.1039/x0xx00000x

www.rsc.org/

HF radiofrequency exposure and/or the presence of carbon nanotubes (CNT) induce modifications to the structure and dynamics of model membranes. These modifications were investigated by multinuclear NMR methods in various phospholipid membrane systems. CNTs were found to spontaneously integrate the superficial layer of membranes at low temperatures; they did not interact with the terminal methyl group of the chains. The local order was increased from C10 to the plateau region of the acyl chain, whereas the local order in the depth was not significantly modified. A specific implication of the choline headgroup was found, resulting in an overall rigidification when CNTs were present. While low-level, athermal radiofrequency exposure in the HF band alone had no significant effect on membrane structure or dynamics, it did partially reverse the consequences of CNT interactions with the membrane by producing a new membrane structure, possibly consistent with gel- or cubic-phase formation.

Introduction

Materials for which at least one dimension is in the nanometer range (typically 1–100 nm) are considered to be nanomaterials. The term covers many systems¹ nanoparticles or ultrafine particles (UFP), they can be natural (volcanic fumes, spray, etc.), produced by human activities such as pollution (heating, transport, etc.) or industrially produced (manufactured nanomaterials)². The nanometric dimensions of these materials confer some specific physical, chemical, electromagnetic, biological (mainly due to high reactivity with proteins) or optical properties^{3,4}. Nanotechnology, developed to produce nanomaterials, has raised numerous scientific and environmental questions^{5–7}. Humans can be exposed to these materials in domestic or occupational settings. Among nanoparticles, carbon nanotubes (CNTs) – cylindrical nanostructures with a length-to-diameter ratio of up to 28 million to 1, and a very large surface area (up to 1000 m²/g)⁸ – have specific mechanistic, electric or thermal properties,

making them particularly interesting for domestic, industrial and military applications. Because CNTs are generally volatile and easily dispersible materials, they are considered to be potentially highly toxic⁹. As both the quality and quantity of CNTs produced increases, it is becoming urgent to determine whether they have any deleterious health effects or raise worries related to public health.

Up to now, although several studies have examined the toxicity of nanomaterials, no definitive conclusions can be drawn with respect to CNTs toxicity. This missing conclusion is mainly due to contradictory results and/or a lack of reproducible experiments using various models. Hence, some studies reported tumour induction and proinflammatory properties (stimulating the production of TNF α , and induction of alveolitis and granulomas) which the authors linked to the formation of free radicals^{10,11}. Conversely, other studies found CNTs to produce no deleterious effects in terms of either radical production or cell survival¹². Membrane diffusion modulation was observed under several experimental conditions, leading several groups to investigate how CNTs interaction with cell membranes^{13,14}.

CNTs behaviour in electrical/electromagnetic environments (EMF) remain incompletely known¹⁵. As these structures exhibit both rad and spikes areas, antenna-like properties causing localised electromagnetic field focusing have been evoked¹⁶.

Self-orientation and forced motions in the EMF have also been evoked and observed (a phenomenon known as CNT radio)

^a Institut de Recherches Biomédicales du Service de Santé des Armées, IRBA, 91223 BRETIGNY-SUR-ORGE, France. Address here.

^b CLINATEC, centre de recherche biomédicale Edmond J. Safra, commissariat à l'énergie atomique et aux énergies alternatives, CEA, 38100 GRENOBLE, France.

^c CHU Michallon, neurosurgery department, 38700 LA TRONCHE, France.

^d DGA Techniques aéronautiques, 47 rue Saint Jean, BP 93123, 31131 Balma Cedex

Electronic Supplementary Information (ESI) available: [details of any supplementary information available should be included here]. See DOI: 10.1039/x0xx00000x

^{16,17}. These observations led to the development of a hypothesis whereby combination of CNTs and EMF would produce synergistic effects. Various mechanisms for these synergistic effects have been suggested. Thus, CNTs could increase/focus EMF interactions; EMF could also increase the toxicity of CNTs, e.g. by enhancing their dispersion in the environment and their capacity to penetrate cells¹⁸.

These hypotheses all involve basic interactions with membranes, and a lack of cellular, metabolic or other active physiological regulation. For this study we therefore used synthetic phospholipid multilayer structures (multilayer vesicles (MLV), dispersions) to mimic the basic membrane structure and dynamics. These models have been extensively used to study membrane interactions with chemicals¹⁹ and physical agents²⁰. The main constituents of most membranes were lecithins, particularly Dipalmitoyl- (DPPC) and Dimyristoyl- (DMPC) phosphatidylcholines. The well-defined bilayer structures that these molecules form, and the physiological relevance of their phase transitions (around 297 K for DMPC, 320 K for DPPC) make these systems suitable for this type of study. To observe the consequences of CNTs, EMF, and CNT/EMF interaction on model membranes, this work used classical liquid NMR methods (¹H-NMR, ³¹P-NMR) and also solid-state-like NMR (²H-NMR, ³¹P-NMR) on natural and d-chain perdeuterated DMPC MLV, in the absence of other possible interactions (i.e., without buffer or protein), in the 293-313 K range, where phase transition occurs.

Materials and methods

Lipids and chemicals

All salts and phospholipids (dimyristoyl-phosphatidyl-choline: DMPC; egg yolk phosphatidyl glycerol: EPG; egg phosphatidic acid: EPA; dimyristoyl-phosphatidyl-serine: DMPS; dimyristoyl-phosphatidyl-ethanolamine: DMPE) were purchased from Sigma-Aldrich (Saint Quentin-Fallavier, France) and were used as-provided. Deuterated solvents and deuterium-depleted water were from Eurisotop (91191, Saint-Aubin, France). Chain perdeuterated DMPC (DMPC-d₅₄) and polar headgroup γ -methyl deuterated (DMPC-d₉) were supplied by Interchim (Montluçon, France).

Carbon nanotubes (CNTs)

Single-wall CNTs from Sigma-Aldrich (sample n°MKBD4057) presented the following purity and characteristics: carbon purity > 90%, i.e., $\geq 70\%$ CNT, 0.7–1.3 nm diameter, with a quality factor of 0.9777, quality factor (Raman) > 94%. CNTs formed aggregate with a mean diameter of 10 μm , as determined by laser granulometry (Horiba Partica LA-950V2) on an aqueous 50 $\mu\text{g}/\text{ml}$ stock sample.

Model membranes

To form small unilamellar vesicles (SUV), chloroformic solutions of phospholipids were first evaporated in a Rotavapor and resuspended in D₂O at a final concentration of

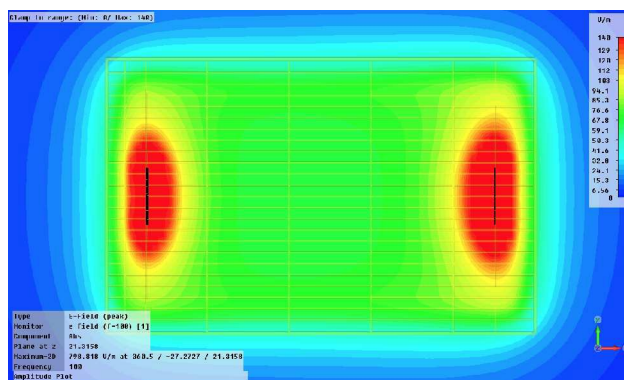


Figure 1: Electric field simulation at 100 MHz

10 mM. SUV were then formed by sonicating the suspension in a sonicating water bath. The size and homogeneity of the SUV were verified by light-scattering and measurement of γ -choline and terminal methyl line widths on ¹H-NMR spectra (see Figure 1).

Multilayer vesicles (MLV) were prepared as DMPC liposomes for ³¹P experiments by successive freeze-thawing cycles to produce a homogeneous milky sample^{21,22}. Suspensions were degassed under nitrogen before transferring to NMR tubes which were then sealed. The final lipid concentration was 50 mM in pure D₂O for ³¹P-NMR. Various W/W proportions of CNT:DMPC were tested by mixing CNT:DMPC in chloroformic suspension before the freezing/thawing procedure. A 2/50 W/W (about 2.10⁻⁴ M/M) was found to be best for the studies performed here. Similar procedures were used to produce multilayers for ²H-NMR experiments, except that 25% DMPC with perdeuterated chains (DMPC-d₅₄) or deuterated headgroup elements (DMPC-d₉) were used to prepare the liposomes¹⁹, and the solvent was deuterium-depleted water. HF-exposed MLV-CNTs were analysed in two groups; spectra for both sham and exposed systems were acquired for the same duration, and acquisition started immediately after the freeze-thawing procedure.

Hydrated samples: To ensure complete hydration of the phospholipids, a weighed volume of D₂O corresponding to 25 times the number of DMPC molecules was added to the tube and mixed with the phospholipids using an antivortex Teflon tip. The tube was then sealed and the sample was allowed to hydrate for 2 days at a temperature where the lipids would remain in the fluid state (300 K). For the samples containing CNTs, a DMPC/CNTs system was prepared as previously²³ and dried before hydration.

Exposure conditions and dosimetry

The exposure device was based on a radiofrequency generator (Marconi 2024, France) connected to a power amplifier (RK A1000, Japan) emitting at 100 MHz. A signal generator (Agilent 33120A, USA) was used to create a modulated square shaped signal at 100 kHz with a duty cycle of 10%. The amplifier was

directly connected to a matched Transverse Electromagnetic (TEM) line specifically designed to ensure a high homogeneity of the electric field between 100 kHz and 500 MHz (vertically polarised plane wave illumination conditions). The field distribution was determined by numerical simulation (Figure 1).

Samples (500 μ l) were loaded into 5-mm quartz NMR tubes. The tube was placed at the middle of the TEM line, in a polystyrene holder known not to interact with electromagnetic field. Depending on their group, samples were then exposed or sham exposed for 1 hour at a power density of 100 W/m². This power density was chosen as it corresponded to twice the ICNIRP-recommended occupational reference level. All experiments were performed at a controlled temperature (295 K). In these conditions, temperature remained stable, as confirmed by the Specific Absorption Rate (SAR) simulation. This stability was in accordance with the very low electromagnetic absorption of water at this frequency.

The SAR was estimated using numerical simulation with the Transmission Line Matrix (TLM) method, implementing Maxwell's equations in the time domain. According to other studies²⁴, TLM is numerically efficiency for SAR computation. In the conditions applied here, the maximal SAR value estimated with the electromagnetic properties of water (permittivity $\epsilon_r = 78$ and conductivity $\sigma = 1.59$ S/m) was around 0.14 W/kg.

NMR experiments

¹H-NMR experiments were recorded at 295 K on a Bruker AVANCE III 400 NMR spectrometer using presaturation of the resonance for water and a spectral width of 10 ppm. Chemical shifts were expressed relative to the resonance for water, set to 4.75 ppm. ¹H-NMR peaks were assigned based on published data and by using basic correlation experiments^{25,26}. Inversion-recovery T1 relaxation experiments were performed using the Bruker software library.

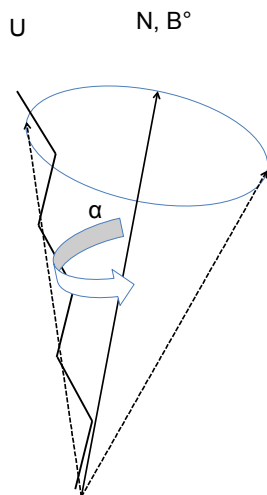


Figure 2: Projected position of main chain axis (U) and normal axis of membrane bilayer (N, B*).

³¹P-NMR experiments were performed at 162 MHz. Phosphorus spectra were recorded using a dipolar echo sequence²⁷:

$$\frac{\pi}{2} - t - \pi - t$$

with a t value of 12 μ sec, a recycling delay of 2 s and composite proton decoupling. Phosphoric acid (85%) was used as external reference. As the chemical shift anisotropy (CSA) measured between low-field shoulder and high-field components were in agreement with published data, and as no isotropic contribution was observed, we considered the contribution of smaller systems (LUV, SUV, micelles) to be almost negligible, and we used the measured values as they stood.

²H-NMR experiments were performed at 61 MHz. Deuterium spectra were recorded using the following quadrupolar echo sequence:

$$\frac{\pi}{2} - t - \frac{\pi}{2} - t$$

with a t value of 15 μ sec and a recycling delay of 4 s.

The free induction decay was shifted by fractions of the dwell time to ensure that its effective time for the Fourier transform corresponded to the top of the echo. The sample temperature was maintained within ± 1 °C by a BVT-2000 unit.

²H-NMR spectra processing: Quadrupolar splitting ($\Delta\nu_Q$) was measured on the spectra after first applying the de-Pake-ing procedure described by Seelig²⁸. From this first fluidity estimation, segmental C–D bond order (S^{CD}) parameters were calculated using the following relation:

$$\Delta V_Q = \frac{3}{4} \cdot A_Q S^{CD} \quad (1)$$

with the static quadrupolar coupling value $A_Q = 167$ kHz²⁹, leading to the simplified formula:

$$S^{CD} = 7,998 \cdot 10^{-3} \times \Delta V_Q \quad (2)$$

where $\Delta\nu_Q$ is expressed in kHz.

The formalism described by Douliez³⁰ was used to extract the C–C bond order parameters (S^{CC}), starting from S^{CC}_{14} (order parameter of the C13–C14 terminal bond of the chain),

$$S^{CC}_{14} = -3.25 \times S^{CD}_{14} \quad (3)$$

and then by using the recurrent relation

$$S^{CC}_i + S^{CC}_{i+1} = -2 S^{CD}_i \quad (4)$$

Although these order parameters are generally considered to be negative³¹, for convenience they were plotted here as positive.

In addition to conformational defects (G defects)³², from the S^{CC} values it was possible to give an estimation of the mean chain length (Lc) - which in fact is an average value as the two chains are perdeuterated - by considering the projection of C-C bonds on the normal to the membrane, N, and static field B⁰ (Figure 2).

By starting from the C-C order parameter S^{CC} ³³:

$$\langle Lc \rangle = \left[\frac{1+(1+8.S_{mol})^{1/2}}{4} \right] \cdot \left[\langle L_{C_n-H} \rangle + \frac{5}{4} \sum_i \left(\frac{1}{2} + \frac{S_i^{CC}}{S_{mol}} \right) \right] \quad (5)$$

with $i=2$ to 14 for DMPC, and where S_{mol} is the molecular order parameter that can be approximated as 1 (since the conic averaging angle, α , tends to 0; see Figure 2), relation (5) can be simplified to:

$$\langle Lc \rangle = 1.75 \cdot \left[\langle L_{C_n-H} \rangle + \frac{5}{4} \sum_i (0.5 + S_i^{CC}) \right] \quad (6)$$

Results

Chain interactions: ²H-NMR of DMPC-d₅₄ dispersions

Quadrupolar splitting

Figure 3A shows a representative spectrum acquired for a dispersion (phospholipid bilayers) of pure DMPC-d₅₄ (dimyristoyl-phosphatidyl-choline with perdeuterated chains) in gel/crystalline phase (at 298 K). The spectral profile

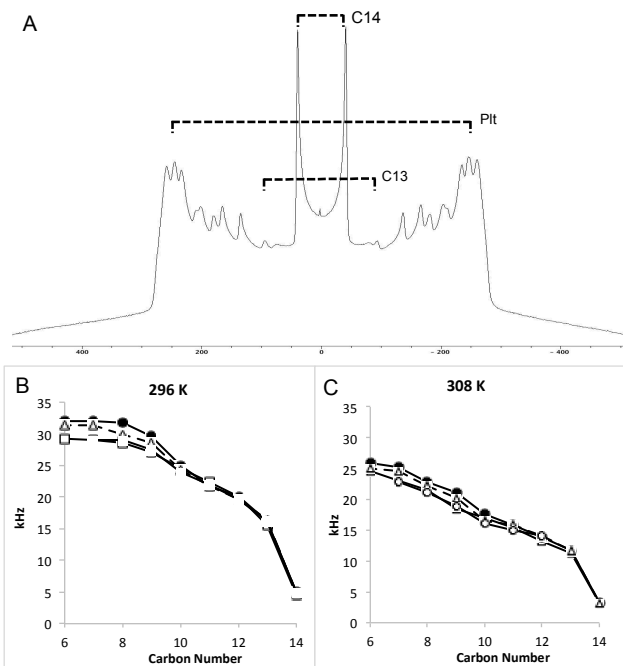


Figure 3: (A) Representative ²H-NMR spectrum of DMPC MLV at the transition temperature. CD₃ and plateau Pake doublets are labelled. Estimation of membrane fluidity at temperatures below 296 K (B) and above 308 K (C). (o) DMPC; (□) DMPC+HF; (●) DMPC+CNT; (Δ) DMPC+CNT+HF.

resembles the superimposition of symmetrical doublets, with each doublet corresponding to a CD₂ group of the acyl chain. For a given doublet, the splitting of $\Delta\nu_Q$ is directly related to the local chain fluidity (see Materials and Methods section). This split can therefore be used as a first approximation as an order parameter. As generally recognised, the fluidity measured for the terminal methyl group, CD₃, is greater than that recorded for methylenic groups close to the polar headgroup (with a 'plateau region' from C2 to C6). The corresponding spectrum (at 298 K) thus includes: (i) an inner doublet with a $\Delta\nu_{Q_{CD_3}}$ of 4 kHz attributed to the CD₃ group; (ii) a succession of doublets with increasing $\Delta\nu_{Q_{CD_2}}$, assigned to the CD₂ group, which extends from C13 to C7; and (iii) an external edge doublet attributed to the deuterium in the C2-C6 plateau region with a $\Delta\nu_Q$ of 29 kHz. Spectra for HF-exposed systems were quite similar. In contrast, in the presence of CNTs, an increase in quadrupolar splitting (increased rigidity) was observed in the most superficial part of the layer, starting from the C10 position, with the split progressively increasing up to the plateau region (Figure 3 B,C). This feature was observed across the whole temperature range considered (293–313 K), and especially around the transition temperature.

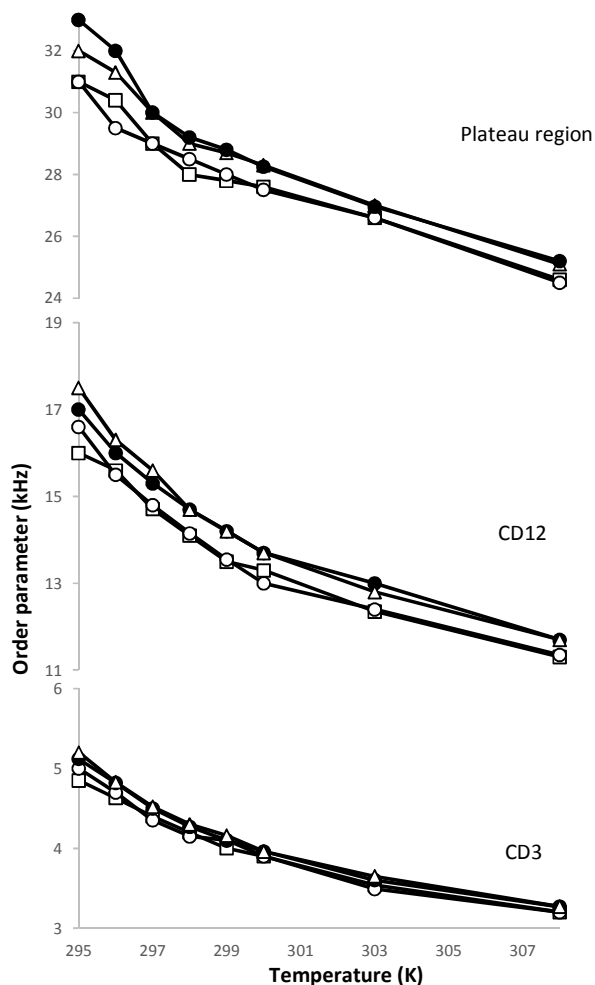


Figure 4: A) Temperature-dependence of S^{CD} measured for C-D bonds, built for terminal methyl, C12 (B), C2-C6 region, Plateau (C). (o) DMPC; (□) DMPC+HF; (●) DMPC+CNT; (Δ) DMPC+CNT+HF.

For instance, the CNT-induced increase of $\Delta\nu_Q$ was measured as 600 Hz (296 K) and 2 kHz (308 K) for the plateau region, and as 400 Hz (296 K) and 1 kHz (308 K) for C12. Interestingly, MLV containing CNTs and exposed to HF displayed smaller differences, but failed to reproduce the initial splitting values measured on pure DMPC. These various quadrupolar splitting values were then used to calculate the carbon-deuterium order parameter, S^{CD} , and to observe its temperature dependence for each level of the chain.

S^{CD} parameters and temperature

Figure 4 illustrates the S^{CD} temperature dependence at several chain levels. For convenience, the differences were recorded directly in kHz, by considering the direct proportionality between the splitting and the order parameters (see Equation 2). As expected, the curves for DMPC clearly showed fluidity to increase with temperature, with a jump at the transition

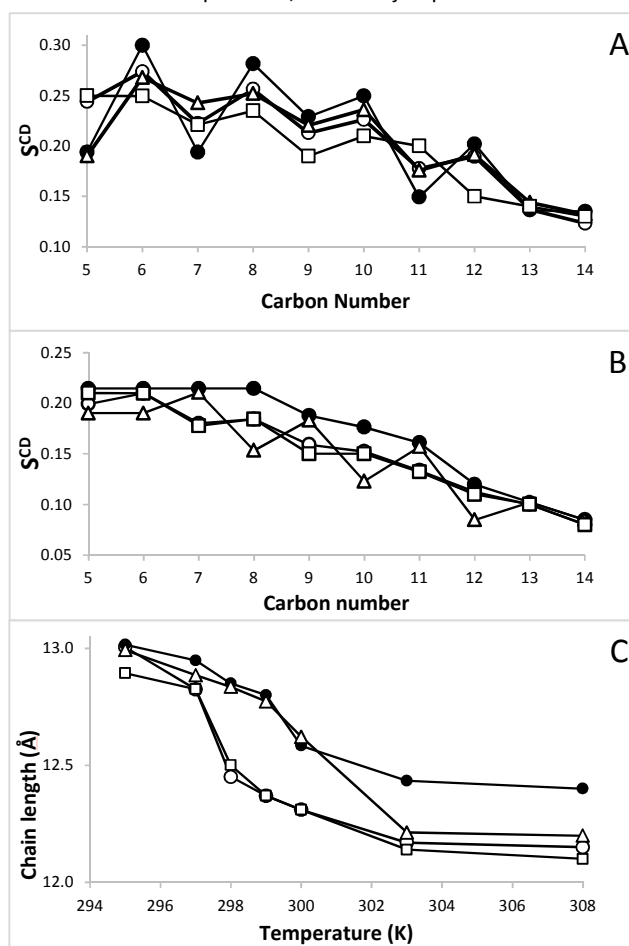


Figure 5: S^{CD} following carbon position, at 295 K (A); 308 K (B) on MLV of (o) DMPC; (□) DMPC+HF; (●) DMPC+CNT; (Δ) DMPC+CNT+HF. C) Mean apparent chain length, estimated on C5–C14 segment.

temperature ($T_i = 297$ K). However, the temperature-induced fluidity increase showed a continuous progression rather than a clear jump at the transition temperature. This observation

was true throughout the length of the chain, up to the terminal methyl level, CD_3 (Figure 4, bottom panel). Conversely, the presence of CNTs led to a membrane fluidity decrease over the whole temperature range, more markedly observed at low temperatures, with the transition appearing almost damped. This feature, present from the C10 level, was more marked in the plateau region (up to 2 kHz at 295 K). In accordance with the results presented above, HF exposure of CNT-containing MLV resulted in a partial recovery of fluidity at low temperatures (1 kHz in the plateau at 295 K; Figure 4, bottom panel).

S^{CC} carbon order parameter and chain length

Figure 5 shows S^{CC} variations as a function of the chain position above (Figure 5A) and below (Figure 5B) the transition temperature^{34–36}. Classically, fluidity increases from the surface to deeper within the layer (CD_3 terminal group), with parity (or odd/even) effects (kick and jog), related to the steric constraints due to the bonds. Our results show that this effect is not observed at the terminal methyl group level.

Low temperatures:

Whereas HF exposure did not modify the odd/even effects, a loss of fluidity was detected over the central part of the layer. This loss of fluidity did not affect the more superficial zone - up to the plateau region. Conversely, CNTs increased the effect of parity (S^{CC} differences of 0.066 versus 0.033 for C5–C6 at 295 K). In addition, simultaneous HF exposure almost completely reversed all the effects observed in the presence of CNTs or HF alone, *i.e.*, the CNTs induced parity and fluidising effects of HF exposure.

High temperatures:

At 308 K the situation was different. While exposure to HF alone had no specific effect, the presence of CNTs resulted in a global increase in rigidity, associated with a loss of odd/even effects. Finally, combined HF/CNTs exposure restored membrane fluidity to control levels. In addition, whereas parity effects were restored and of similar intensity to that in DMPC, they were found to be inverted.

As these results evoked possible alteration of chain conformations, it was of interest to investigate the average effective chain length. Note that the rough estimation obtained by applying Equations (5) and (6) was limited due to the fact that the DMPC was perdeuterated on the two chains, and that the two chains differed in length and dynamics (Figure 5C). Once again, HF exposure had no effect on the chain length and temperature dependence of pure DMPC systems; and the presence of CNTs did not modify the chain length at low temperatures. In contrast, increased lengths were observed at high temperatures (0.4 Å at 308 K), rising to a maximum of 0.5 Å at 309 K.

The interactions between physicochemical agents, besides chain implication, also involved a surface contribution at the

level of the polar headgroup. This contribution influences both the binding and structural dynamics of the membrane.

Polar head interactions: DMPC dispersions based on ^{31}P - ^2H -NMR

Influence of composition of the polar headgroup. ^{31}P -NMR

Dispersions of various phospholipids (DMPC, DMPE, DMPS at 50 mM) were used to assess how the polar headgroup affected membrane interactions with CNTs, and HF used either alone or simultaneously, by recording ^{31}P -NMR spectra in the 291–313 K temperature range.

DMPC

It is important to recall that the chemical shift for phosphorus differs depending on how the nucleus is oriented in the field, due to shielding, and that the global spectrum reflects the distribution and dynamics of all orientations present in this case. Thus, in membranes, the ppm difference between the low-field and high-field edges of the spectrum is known as CSA and is related to the membrane's fluidity at the polar head level, where the phosphorus is located. Hence, fast-reorienting mobile phosphorus gives very resolved peaks (several Hz), *e.g.*

in small micellar systems or true solutions. Conversely, phosphorus nuclei in solid-state only give an extremely broad and unresolved resonance (more than 100 ppm). In addition, motional averaging (which will reduce CSA) occurs in membranes, and is known to increase with temperature, with a jump at the temperature at which a transition between gel and liquid crystal phases occurs (297 K for DMPC; see Figure 6D)³⁷. Hence, CSA temperature dependence is a good way to approximate membrane dynamics at this level, while the overall line shape can be used to explore the overall membrane structure and organisation (bilayer, hexagonal phase or isotropic contribution, etc.). The ^{31}P -NMR spectrum recorded for MLV composed of DMPC (Figure 6A) was typical of an axially symmetrical structure, and displayed CSA at 65 ppm, which is classically related to a gel/crystalline phase³⁸. As the CSA measured between the low-field shoulder and the high-field component were in agreement with previously reported data, and as no isotropic contribution was observed, we considered that the contribution due to smaller systems (LUV, SUV, micelles) was almost negligible, we therefore used the measured values without correction.

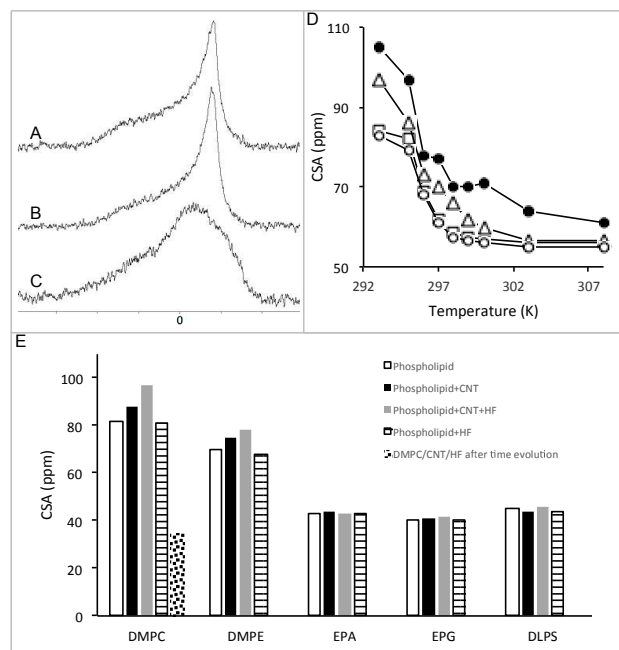


Figure 6: ^{31}P -NMR spectra recorded at 295 K on MLV of pure DMPC (A) and in the presence of CNT (B). (C) same as B after 2 days of evolution. (D): plot of CSA as function of temperature built from (○) DMPC; (□) DMPC+HF; (●) DMPC+CNT; (Δ) DMPC+CNT+HF. (E): CSA values at 295 K from MLV of various phospholipids (□) pure; (■) with HF; in the presence of CNT (▨); HF and CNT (=); second phase from DMPC/CNT/HF after time evolution (:::).

As described above, MLVs composed of DMPC exhibited CSA with a decrease of about 30 ppm in the 295–313 K range and a transition at 297 K. A relatively similar progression was found after HF exposure. Conversely, the presence of CNTs strongly reduced membrane fluidity (with the difference exceeding 25 ppm at low temperatures; see Figure 6D). However, neither the main bilayer structure nor the transition temperature were affected. Indeed, membrane disruption would have resulted in the appearance of an isotropic peak at 0 ppm. Furthermore, while the time-course (2 days) did not affect pure DMPC

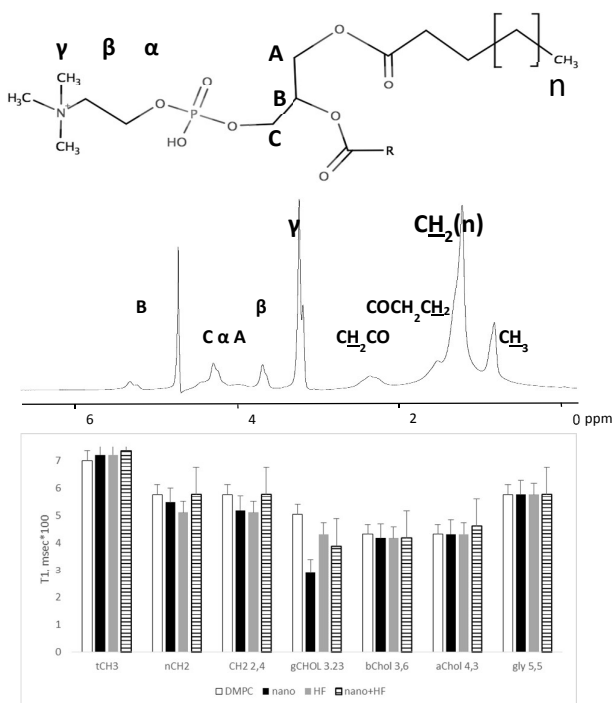


Figure 7: (A) DMPC proton nomenclature: $n=12$; $R=C_{14}H_{29}$. (B) $^1\text{H-NMR}$ spectrum for pure DMPC SUV at 298 K. (C) T_1 values calculated for the different building blocks of DMPC (□) pure; (■) with HF; (▨) in the presence of CNT; (=) combined HF and CNT exposure.

membranes, the spectra for CNT-containing systems showed a second phase, subtracted from the main structure (Figure 6C). This phase, while isotropic, was too broad (40 ppm) to be attributed to the formation of micelles or any overall detergent effect, rather than to other non-oriented structures (cubic phase, gel phase, etc.). These features were not observed when DMPC/CNT systems were exposed to HF, in which case the rigidifying effect was clearly limited (15 ppm at 295 K) but the transition temperature was unchanged.

Other phospholipids

No such modifications were observed when other phospholipids were used to produce MLV models (Figure 6E). Only a limited increase in CSA was measured with MLV composed of DMPE also containing CNTs (about 2 ppm), and no other modification was noted upon coexposure or exposure to HF alone.

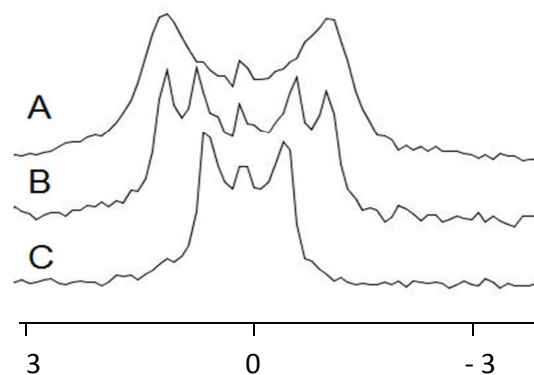


Figure 8: $^2\text{H-NMR}$ (ppm) spectra for perdeuterated γ -choline (N-trimethyl) DMPC at 308 K. Spectra are for pure MLV (A), MLV in the presence of CNT (B), MLV containing CNT after 1 h HF exposure (C).

SUV composed of DMPC were then used to investigate the relaxation parameters at different levels within the membrane, pure SUV were compared to SUV with CNTs and/or HF-exposed SUV.

Relaxation measurements in SUV composed of DMPC: $^1\text{H-NMR}$

Due to their small diameter (20 nm), SUV give rise to relatively well-resolved $^1\text{H-NMR}$ that can be observed by classical liquid NMR methods. T_1 values were not significantly modified upon incorporation of CNTs or exposure to HF (less than 5% variation; Figure 7), except for the chain's methylene protons ($n\text{CH}_2$, 1.26 ppm and CH_2 , 2.4 ppm) for which 8% variations were recorded (HF: 570 ms; CNT: 520 ms; CNT + HF: 512 ms)²⁵.

In contrast, almost 2-fold variations in T_1 were measured for N-trimethyl choline (γ : 3.23 ppm) (DMPC without exposure: 505 ms; DMPC + CNT: 289 ms; DMPC + HF: 390 ms). The variation was limited in the coexposure condition (DMPC + CNT + HF: 430 ms).

$^2\text{H-NMR}$ of DMPC- d_9

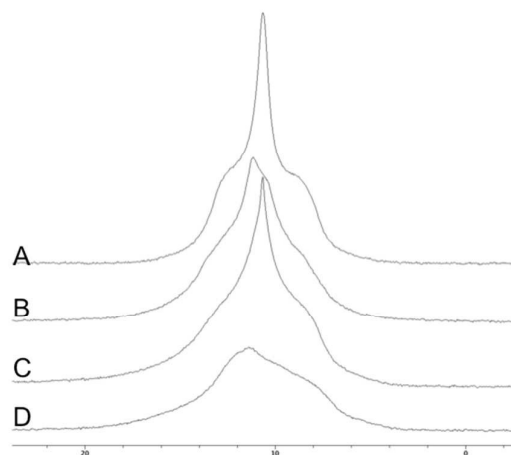


Figure 9: $^2\text{H-NMR}$ (ppm) spectra of γ -choline perdeuterated DMPC (N-trimethyl) at 308 K, pure (A) and in the presence of NTC (B); same as B with 1 h HF exposure (C).

To assess how the trimethyl choline group contributes to interactions with the MLV, dispersed DMPC perdeuterated on the γ -choline group were observed by $^2\text{H-NMR}$.

As the γ -protons of a choline headgroup are magnetically equivalent, a single doublet with a quadrupolar splitting of 2 kHz was detected, in agreement with the relatively rapid reorientation of this group in the field. Hydration water in excess was also identified as a single central peak (Figure 8A). The presence of CNTs results in a more mobile population (1.4 kHz), which appears at the expense of the initial population (Figure 8B). Two distinct phases were present, and linewidths of less than 100 Hz were measured, confirming that the whole system is relatively mobile. As above, HF exposure alone did not induce any significant spectral changes compared to the reference spectrum (data not shown); in contrast, coexposure (CNTs + HF; Figure 8C) increased the contribution of the more mobile phase, while simultaneously reducing the reference spectrum compared to Figure 8A.

Involvement of polar head hydration

In a fully D_2O -hydrated system, the $^2\text{H-NMR}$ spectrum for DMPV MLV appears as the sum of two components: (i) isotropic resonance corresponding to free water in excess (linewidth: 70 Hz), and (ii) a doublet with a quadrupolar splitting of 250 Hz, which is related to water immobilised on the polar headgroup (Figure 9A). When CNTs are incorporated into the membrane (Figure 9B), a third component appears at 120 Hz (QS). HF exposure alone (Figure 9D) completely abolished the isotropic contribution, while the relatively broad resonance (400 Hz QS) evoked the presence of a proportionally less mobile structure. The same observation was made in coexposure conditions, which produced an intense isotropic line.

Discussion

The goal of the present work was to detect any alterations to membrane structure and/or dynamics upon coexposure to two environmental agents - electromagnetic fields and carbon nanotubes. Synthetic membranes were used to avoid any specific or active cellular mechanisms and to allow general modes of interaction to be observed at permissible exposure levels, as defined for the general population and specific occupations (communications, military, etc.)^{1,39}. The hypothesis that interactions with these agents could combine (to produce additive, synergistic or antagonistic effects) was previously proposed by numerous scientific groups. Considering the importance of surface interactions and also the strong hydrophobic properties of CNTs, this study attempted to distinguish between the main membrane domains: the hydrophobic chains embedded under the surface; and the superficial, charged polar headgroups, which are directly exposed to the medium.

Acyl chains

Using perdeuterated chains and $^2\text{H-NMR}$ it was possible to study the dynamics and derive structural information from the same spectrum. Interestingly, analysis of the fluidity profiles (QS) and how they were affected by temperature showed no alteration of either the main bilayer structure or the transition temperature under the experimental conditions used. However, CNTs enhanced the QS of the superficial part of the chain (starting from C10) across the whole temperature range. In contrast, HF exposure alone had no effect, but HF/CNT coexposure limited the CNT-induced modifications. This result was consistent with electron spin resonance data for spin-labelled fatty acids integrated into the membrane (not shown). Calculation of the C–D bond order parameters (S^{CD}) for CNT-containing MLV indicated rigidification of the ‘plateau’ region at low temperatures, which was partially corrected by simultaneous HF exposure. Finally, the dynamics and geometric information on the main carbon skeleton were obtained by calculating the C–C bond order parameter (S^{CC}). Besides a local order increase at low temperatures in the presence of CNTs, which was partially corrected by HF coexposure (as for S^{CD}), the parity effects (aka odd/even effects) were also enhanced in the superficial part of the membrane. This variation was also limited by coexposure to HF, although HF alone had only very limited effects and did not alter the local geometry. At high temperatures, HF exhibited no greater effect. Conversely, while the CNTs still induced a local order increase, overall parity effects were completely lost and the mean chain length was increased. Furthermore, the HF/CNT combination restored both apparent chain length and fluidity, and the odd/even effects were inverted.

These features strongly suggest that CNTs at least partially integrate the membranes, although they do not affect the deepest part of the layer. This result is in agreement with the fibrous structure and hydrophobic properties of CNTs. CNTs could align with the chain, integrating as neighbouring elements in the membrane, causing a certain degree of rigidity that can best be observed close to the membrane’s surface. These types of interactions clearly differ from those observed with other small hydrophobic molecules such as steroids or cholesterol. In these other cases, although the local order is magnified in the superficial region of the chain, the relative proximity in the deeper part of the layer (beyond the C27 chain end of cholesterol) results in an increased fluidity³². S^{CC} variations give a good illustration of the CNT-induced steric constraints³³. Besides the fluidity effects observed on QS and S^{CD} , both enhancement of parity effects (normally present in a bilayer, related to normal asymmetry of sn-1 and sn-2, kick/jog) and an increase in chain length were observed. These features may be related to stretching and loss of conformational freedom, which could themselves be related to steric hindrance at low temperatures. Partial desorption would also explain the disappearance of these modifications and the loss of parity effects at high temperatures is possibly related to a local vacuity induced by CNT motion.

HF exposure

The exposure level used ($100 \text{ V/m} = 25 \text{ W/m}^2$) does not induce any thermal effect, as attested by the absence of effect on order parameters, transition temperature, chain length or parity upon HF exposure alone. Conversely, CNT-induced modifications were limited when membranes were exposed to HF. This reversal could be due to local thermal agitation; however, this explanation would not be consistent with the lack of the effect of HF alone.

The electrical properties of CNTs suggest another basis for CNT/membrane/HF interactions. CNTs may be considered as potential antennae (spike effects) that can themselves self-orient in an electromagnetic field; in other words, a nanotube placed in an electric field focuses the field through its tip. As the spike is very thin, emission can occur even with very small potentials ("field emission")^{40,41}. The result is a local mechanical HF-related vibration. Moreover, the orientation of CNTs in the field agrees well with the observed local structural modifications, S^{CC} parameters, and chain length at high temperatures. In these conditions, rather than the usual (entropic) thermally-induced increase in fluidity, new constraints are present, consistent with inversion of the parity effects on S^{CC} . Several publications also report that such effects can be amplified by forcing the CNTs to oscillate at the HF transmitter frequency^{16,17}.

Polar heads

The ^{31}P -NMR results of DMPC dispersions agree with those obtained from chain study: neither the transition temperature nor the main bilayer structure is modified. CNT-induced rigidity was noted across the whole temperature range, and could be partially corrected by exposure to HF. HF exposure was sufficient to reverse this effect of CNTs; however, a time-course for the CNT/MLV system revealed another structure. The relatively broad component identified at the isotropic position appears to be related to a more symmetric and viscous system, evoking unusual phases (gel, cubic, amorphous, etc.), and excludes any detergent effect or formation of mobile micelles^{42,43}. This type of progression was not detected upon exposure to HF.

MLV built with other phospholipids differed in their polar headgroup (serine, glycerol, acid) and exhibited no clear interaction with either CNTs or HF, except for ethanolamine (DMPE). However, with this compound no changes were detected over time and no new structures formed.

T_1 relaxation measurements showed a strong interaction between CNTs and the γ -methyl groups of DMPC. Conversely, no modification was detected in the choline (or ethanolamine, not shown) methylenic groups. Furthermore, ^2H -NMR observation of γ -methyl-perdeuterated DMPC revealed a second component with enhanced mobility. Although HF alone induced no modification, upon combined exposure to CNTs plus HF, this structure - initially the sole component - completely vanished. (Deuterated) water hydration was

investigated by ^2H -NMR. The reference spectrum consisted of a resolved central line corresponding to excess free water superimposed on the doublet representing bound water. In the presence of CNTs, a second doublet appeared with a smaller between-peak distance than that of the reference hydration water, suggesting an increase in fluidity or the exchange rate. HF exposure alone produced a broad unresolved resonance without detectable free water, indicating a viscous system. Coexposure to CNTs/HF partially restored the native structure, but a free water-containing three-component spectrum, was still recorded.

Interactions between CNTs and zwitterionic phospholipids (mainly choline and less markedly ethanolamine) appear preferential although not specific. In these cases, CNTs induced the formation of a new phase, which was either immediately detectable (^2H) or appeared after some time (^{31}P). As with the chains results, while ^{31}P spectra were not affected by HF exposure alone, HF/CNT coexposure could prevent the rigidity induced by CNTs, thus a gel was not formed. These results could not be explained by a simple mechanical tumbling. Moreover, both the HF effects on the hydration water and the detection of new structures at γ -choline level are consistent with structural rearrangements at the water-membrane interface involving phosphorus nuclei, water and choline groups. These types of interactions are normally present in the membranes, and would be stabilised by CNTs.

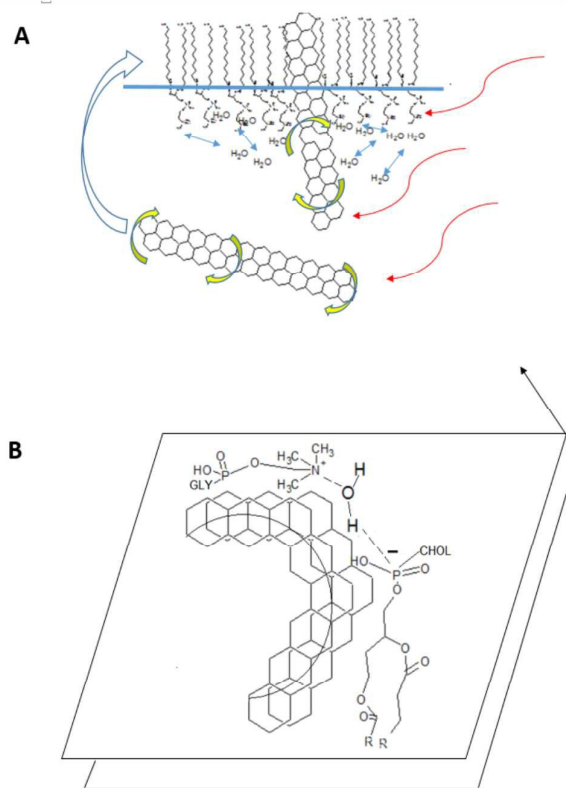


Figure 10: (A) Attraction, tumbling and incorporation of CNT throughout the layer and HF interaction with water (arrows); (B) molecular hydrogen bonding due to hydrogen bonds forming with water molecules, in a cross-section of the route parallel to the membrane's surface.

HF could then interact with this newly-formed structure, both geometrically and through electrical interactions with the CNTs themselves. This point will be developed in the Appendix below, where we present some directions for future studies.

CONCLUSIONS

This study showed that, in the absence of any active biological process (as is the case in model membranes (MLV)), CNTs could interact relatively specifically at the membrane surface with choline headgroups, and also deep within the layer without reaching the interlayer region of the bilayer. In addition, in the absence of any thermal effect and of modifications induced by HF alone, coexposure could limit and modify the consequences of the presence of CNTs. This was especially true for the interactions at the polar head level, where molecular rearrangements and the formation of new structures can reasonably be suspected. Such interactions should involve the electromechanical properties of CNTs (see Appendix). The next step will be to investigate CNT/membranes exposed to HF in living biological systems where charge motion, active ionic fluxes and metabolic regulation play essential roles.

Appendix: mechanistic hypotheses for CNTs/HF interactions within membranes

In the interactions investigated in this paper, four protagonists can be easily identified:

- The membrane phospholipids, which can be split into their two constituent building blocks:
 - the polar headgroup (glycero-phosphocholine);
 - and the two hydrophobic acyl chains;
- CNTs, hydrophobic, electrical conductors and receptors, with a very extensive accessible surface area known to magnify intermolecular interactions;
- HF, presumed to interact with conductors, charged and/or linear systems.

CNTs and DMPC: hydrophobic interactions are short-ranged, but collaborative. It is highly likely that CNT-surface interactions occur as linear contact with chains would be energetically favourable (Figure 10). Such interactions between apolar molecules and membranes have previously been shown to be strong enough to extract phospholipids from membranes: such as with cyclodextrin-induced extraction of phosphatidyl inositol from membranes. Moreover, this extraction was found to be specific to the inositol polar headgroup, similar to the findings described here for choline phospholipids. However, this hypothesis can be refuted by considering that the transition temperature of the main bilayer structures, in both ^{31}P - and ^2H -NMR, was not qualitatively affected by the presence of CNTs, and that no isotropic

component was observed. These results indicate that no free-moving phospholipids, e.g. aggregates or micelles, were present.

However, CNTs are highly likely to integrate the surface and the external part of the layer. The involvement of the polar headgroup in this incorporation is also obvious, as are the contributions of phosphorus, γ -choline and hydration water. Conversely, the absence of modifications to the spectroscopic properties of α,β -choline and glycerol suggest that molecular rearrangements occur at the reactive group level. Hydrogen bonding through water molecules has been extensively reported (ref ici). Based on this, as not all the headgroup components are involved, linear bonding along the CNTs' axis is unlikely to occur. Conversely, lateral displacement of the polar headgroup must occur, due to the geometric steric hindrance conferred by the CNT "rod" itself (diameter of about 0.1 nm). Stabilisation may be obtained around the circumference of the CNTs.

High frequency

The power level used does not induce any thermal or direct interaction with the membrane itself. Conversely, the membrane's water hydration appears to be clearly modified, based on the simultaneous observation of a broad, poorly resolved, resonance (^2H -NMR of hydration water) and the disappearance of the free water component. These effects both support systems which are more immobilised and/or capable of exchange with intermediate kinetics. This point was confirmed by modifications to the observation field (NMR frequency) and temperature (not shown).

HF and CNTs: HF electromechanical interactions with CNTs are clearly consistent with the partial removal of CNTs from the membrane, as observed by the partial recovery of the structure upon coexposure. However, the new phase detected by the ^2H -NMR hydration study reveals a structure which is more stable overall – bordering on amorphous – and in dynamic equilibrium. This structure could stabilise the arrangement induced by CNTs alone, either partially (^2H -hydration observations) or completely (DMPD- d_9 experiments).

Notes and references

- 1 Royal Society (Great Britain) and Royal Academy of Engineering (Great Britain), *Nanoscience and nanotechnologies: opportunities and uncertainties*, Royal Society : Royal Academy of Engineering, London, 2004.
- 2 A. Helland, P. Wick, A. Koehler, K. Schmid and C. Som, *Environ. Health Perspect.*, 2007, **115**, 1125–1131.
- 3 R. J. Chen, Y. Zhang, D. Wang and H. Dai, *J. Am. Chem. Soc.*, 2001, **123**, 3838–3839.
- 4 A. Bianco, K. Kostarelos, C. D. Partidos and M. Prato, *Chem. Commun. Camb. Engl.*, 2005, 571–577.

- 5 C.-W. Lam, J. T. James, R. McCluskey, S. Arepalli and R. L. Hunter, *Crit. Rev. Toxicol.*, 2006, **36**, 189–217.
- 6 T. A. Kuhlbusch, C. Asbach, H. Fissan, D. Göhler and M. Stintz, *Part. Fibre Toxicol.*, 2011, **8**, 22.
- 7 A. Kumar and A. Dhawan, *Arch. Toxicol.*, 2013, **87**, 1883–1900.
- 8 X. Tan, C. Lin and B. Fugetsu, *Carbon*, 2009, **47**, 3479–3487.
- 9 F. Mouchet, P. Landois, E. Flahaut, É. Pinelli and L. Gauthier, *Environ. Risques Santé*, 2009, 047–055.
- 10 A. Peigney, C. Laurent, E. Flahaut, R. R. Bacsa and A. Rousset, *Carbon*, 2001, **39**, 507–514.
- 11 S. B. Lovern and R. Klaper, *Environ. Toxicol. Chem.*, 2006, **25**, 1132–1137.
- 12 I. Fenoglio, M. Tomatis, D. Lison, J. Muller, A. Fonseca, J. B. Nagy and B. Fubini, *Free Radic. Biol. Med.*, 2006, **40**, 1227–1233.
- 13 I.-C. Yeh and G. Hummer, *Proc. Natl. Acad. Sci. U. S. A.*, 2004, **101**, 12177–12182.
- 14 A. A. Shvedova, E. R. Kisin, R. Mercer, A. R. Murray, V. J. Johnson, A. I. Potapovich, Y. Y. Tyurina, O. Gorelik, S. Arepalli, D. Schwegler-Berry, A. F. Hubbs, J. Antonini, D. E. Evans, B.-K. Ku, D. Ramsey, A. Maynard, V. E. Kagan, V. Castranova and P. Baron, *Am. J. Physiol. - Lung Cell. Mol. Physiol.*, 2005, **289**, L698–L708.
- 15 D. Pantarotto, J.-P. Briand, M. Prato and A. Bianco, *Chem. Commun.*, 2004, **0**, 16–17.
- 16 K. Jensen, J. Weldon, H. Garcia and A. Zettl, *Nano Lett.*, 2007, **7**, 3508–3511.
- 17 C. Rutherglen and P. Burke, *Nano Lett.*, 2007, **7**, 3296–3299.
- 18 S. Barrau, P. Demont, E. Perez, A. Peigney, C. Laurent and C. Lacabanne, *Macromolecules*, 2003, **36**, 9678–9680.
- 19 M. A. Parker, V. King and K. P. Howard, *Biochim. Biophys. Acta BBA - Biomembr.*, 2001, **1514**, 206–216.
- 20 B. B. Bonev and M. R. Morrow, *Biophys. J.*, 1995, **69**, 518–523.
- 21 M. Roux, T. Huynh-Dinh, J. Igolen and Y. Prigent, *Chem. Phys. Lipids*, 1983, **33**, 41–45.
- 22 E. Schechter, 1990.
- 23 G. Laroche, E. J. Dufourc, J. Dufourcq and M. Pézolet, *Biochemistry (Mosc.)*, 1991, **30**, 3105–3114.
- 24 A. Laisné and J. Drouet, *CEM*, 2014.
- 25 J. M. Neumann, A. Zachowski, S. Tran-Dinh and P. F. Devaux, *Eur. Biophys. J.*, 1985, **11**, 219–223.
- 26 J.-C. Debouzy, D. Crouzier, F. Bourbon, M. Lahiani-Skiba and M. Skiba, *J. Drug Deliv.*, 2014, **2014**, 575719.
- 27 T. Mavromoustakos, I. Daliani and J. Matsoukas, *Bioact. Pept. Drug Discov. Des. Med. Asp.*, 1999, **22**, 13–24.
- 28 J. Seelig, *Q. Rev. Biophys.*, 1977, **10**, 353–418.
- 29 G. Zaccai, J. K. Blasie and B. P. Schoenborn, *Proc. Natl. Acad. Sci.*, 1975, **72**, 376–380.
- 30 J.-P. Douliez, A. Léonard and E. J. Dufourc, *J. Phys. Chem.*, 1996, **100**, 18450–18457.
- 31 M. Hong, K. Schmidt-Rohr and A. Pines, *J. Am. Chem. Soc.*, 1995, **117**, 3310–3311.
- 32 J. Pailler, A. Gadelle, F. Fauvelle, V. Dabouis, D. Crouzier and J. Debouzy, *J. Drug Deliv. Sci. Technol.*, 2005, **15**, 419–426.
- 33 J.-C. Debouzy, D. Crouzier and A. Gadelle, Elsevier, 2007, vol. 65, pp. 331–341.
- 34 H. Schindler and J. Seelig, *Biochemistry (Mosc.)*, 1975, **14**, 2283–2287.
- 35 D. Huster, K. Arnold and K. Gawrisch, *Biochemistry (Mosc.)*, 1998, **37**, 17299–17308.
- 36 J. Lu, Miami University, 2007.
- 37 S. Mabrey and J. M. Sturtevant, *Proc. Natl. Acad. Sci. U. S. A.*, 1976, **73**, 3862–3866.
- 38 E. J. Dufourc, C. Mayer, J. Stohrer, G. Althoff and G. Kothe, *Biophys. J.*, 1992, **61**, 42–57.
- 39 International Commission on Non-Ionizing Radiation Protection, *Health Phys.*, 2004, **87**, 187–196.
- 40 S. I. Cha, K. T. Kim, K. H. Lee, C. B. Mo, Y. J. Jeong and S. H. Hong, *Carbon*, 2008, **46**, 482–488.
- 41 J. Mintmire and C. White, *Phys. Rev. Lett.*, 1998, **81**, 2506.
- 42 D. G. Gorenstein, *Phosphorous-31 NMR: Principles and applications*, Academic Press, 2012.
- 43 D. G. Gorenstein, *eMagRes*.